Environmental Protection Research
https://ojs.wiserpub.com/index.php/EPR/

UNIVERSAL WISER PUBLISHER

Research Article

Evaluating Dry and Wet Season Precipitation from Remotely Sensed Data Using Artificial Neural Networks for Floodplain Mapping in an Ungauged Watershed

Abhiru Aryal, Amrit Bhusal, Ajay Kalra*

School of Civil, Environmental and Infrastructure Engineering, Southern Illinois University, Carbondale, USA.
E-mail: kalraa@siu.edu

Received: 19 December 2022; **Revised:** 10 February 2023; **Accepted:** 27 February 2023

Abstract: This research creates a framework for modelling the rainfall-runoff process using satellite precipitation data and a floodplain map in ungauged urban watersheds. The combined effects of urbanisation and climate change over the past few decades have increased the number of flooding incidents. Accurate prediction of the flood-prone zone is crucial for policymakers and system managers to build the watershed's resilience during catastrophic flooding events. Precipitation and runoff data are crucial for hydraulic and hydrologic analysis and for identifying flood-prone areas. However, it is difficult to obtain precipitation and discharge data for hydrologic analysis in data-scarce regions. In this context, this research employs satellite precipitation products for rainfall-runoff analysis, which is subsequently utilised in a hydraulic model to delineate a flood-prone zone in an ungauged watershed. The Hydrologic Engineering Centre-River Analysis System (HEC-RAS) and Hydrologic Modelling System (HEC-HMS) models were utilised in the study region to simulate and analyse interactions between rainfall, runoff, and the extent of the flood zone. Setting up and calibrating the HEC-HMS model using a satellite precipitation product is required for the dry and wet seasons. For the wet and dry seasons, HEC-HMS gets validated with an R-square value of 0.72 and 0.85, respectively. Three types of simulations were conducted in the calibrated HEC-HMS model to create the hydrograph with 25-, 50-, and 100-year of rainfall return periods. Finally, the one dimensional HEC-RAS model generates a flood inundation map for the pertinent flooding occurrences from the acquired peak hydrograph. By comparing the values of the specified return periods, the produced flood map depicts the affected area during various return periods of flooding events and provides a quantifiable display of inundation extent percentage (IE%).

***Keywords*:** precipitation estimation from remotely sensed information using artificial neural networks-climate data record (PERSIANN-CDR), HEC-HMS, HEC-RAS, flood, inundation extent

1. Introduction

According to the Intergovernmental Panel on Climate Change (IPCC), studies from 1951 to 2012 concluded that the global temperature increased by 0.8 to 0.14 °C [1]. Climate change has increased droughts, uncertain precipitation, and flooding [2, 3]. Thus, climate change may cause more precipitation and frequent rises in water levels in many places than they used to be, while in some places it may cause more drought [4]. The simple and general reason is that the more the temperature rises, the higher the evaporation rate, increasing the frequency of rainfall and more flooding events.

DOI: https://doi.org/10.37256/epr.3120232255

Moreover, the melting and evaporation of the accumulated snow also change the precipitation pattern. In the western part of the United States (US), due to the warmer climate, the hydrology has altered, resulting in the alteration of snow and rainfall, which resulted in a decrease in spring-summer flow [5]. With a high precipitation measurement, the US has a 24% incremental storm count. Also, there has been colossal damage around the US due to floods in the 20th century. The northeast's extreme condition after Hurricane Sandy is evidence of what the future might hold and what will happen to the communities built over the floodplain. Furthermore, the damages in the Midwest are the result of the 100 and 500 years return period floods. So, even the smaller creeks in the Midwest are getting flooded. The catastrophic floods are destroying settlement areas and increasing pollution in the downstream area, degrading the water quality and public health. There is also the shrinkage of water supplies due to the shift in rainfall patterns and increasing temperatures [6]. As a result, proper planning of the settlement around the rivers is necessary, so the inundation analysis of various rivers and creeks is crucial to see their risk factors.

Determining inundation extent has been the primary goal for the water resources planners and policymakers, as such studies are crucially important for developing the proper management plan to start the new structuring of the residential areas or developing new policies of protection [7-9]. There are many rivers and creeks in the US whose watersheds will not have meteorological stations within their watersheds, so the precipitation data required for hydrology and hydraulic modelling can be extracted in various other ways. One of the methods accepted in this study is extracting the precipitation data from Precipitation Estimation from Remotely Sensed Information using Artificial Neural Networks (PERSIANN). The study cannot begin with the extraction of precipitation because getting the runoff primarily depends on the precipitation and other parameters, like land use and soil type [10]. To extract the runoff for multiple land use and soil type parameters using Geographic Information System (GIS) extensions, the Hydrologic Engineering Centre-Hydrologic Modelling System (HEC-HMS) is used. Finally, the hydraulic modelling in the Hydrologic Engineering Centre-River Analysis System (HEC-RAS) generates the floodplain. So, this study is based on the physical model coupling HEC-HMS and HEC-RAS in the ungauged watershed. Different return periods might have different floodplains; thus, their comparative study shows an increasing or decreasing risk factor. Several past and present studies show that the GIS is appropriate for the mapping of flood plains at various stages and presenting various flood zones [11].

There are several theories on applying the PERSIANN system and case studies in different areas. The study of the event of Hurricane Katrina in 2005 shows the good spatial coverage of PERSIANN-Climate Data Record (CDR). The study of the 1986 Sydney flood in Australia supports the good estimation of the PERSIANN-CDR precipitation [12]. In addition to the comparative study in East Asia and the Taklamakan desert, when comparing precipitation indices of different percentiles with the gridded precipitation data, PERSIANN holds better validity in the extreme monsoon region than in a dry climate. However, the gridded data can also be scattered [13]. Furthermore, a comparative study of the rainfall prediction model across the central US PERSIANN shows better estimation than others. However, it needed to give better volumes during extreme events [14]. The current study aims to use the PERSIANN system when the watershed is ungauged and show the validation of the model for each separate season.

The framework developed for any study is useful for a similar approach to generating the required floodplain. In several approaches, the model is verified for either dry season or wet season rainfall. Many studies have shown the validity of the HEC-HMS model for any single-season dataset [15]. Then the floodplain is generated directly using HEC-RAS or CivilGeo HEC-RAS [16]. The approximate validation of the model for the rainfall of both seasons is believed to predict a more reliable floodplain. The effectiveness and dependability of the model may be adequate given the seasonal variation in rainfall [17]. The water availability fluctuates in the wet and dry seasons, so the model validation of precipitation data for both seasons is adequate [18]. Considering precipitation data from both seasons improves flood forecasting by removing systematic errors [19]. Including precipitation data from all seasons when representing runoff in the HEC-HMS model enhances the accuracy and dependability of floodplain approximations and projections. After the first simulations, if the parameters considered for checking the accuracy are not within the defined limit, then the rainfall-runoff model is optimised using the optimisation tools in HEC-HMS. The optimising parameters in the rainfall-runoff model are the curve number (CN), initial abstractions, lag time, Muskingum coefficient K, and x value. Following optimization, the parameters for checking accuracy are checked again, and the value must be within the limit to be considered validated and used for further processing. For applying the runoff from HEC-HMS, HEC-RAS is modelled to present the flood plain. The parameter to optimise the HEC-RAS model is Manning's coefficient. Once

the model is optimised and gets validated by checking accuracy parameters, the floodplain it generates can be utilised for further processing. The floodplain can be directly presented in the two dimensional analysis, considering the time series data [20]. Climate data is typically taken into account when predicting the floodplain using projected flow values in most studies [21]. Considering the climate model, the scenario is sometimes different and projects drought conditions [22]. Therefore, the portrayal of hydro-climatic co-variability shows the variability of impact on water resources [23, 24]. Compared to the machine learning model, the rainfall-runoff model (HEC-HMS) predicts better values [25]. The Artificial Neural Network (ANN) model is also considered in rainfall-runoff simulation [26]. The Support Vector Machine (SVM) framework's projected precipitation is considered to be more dependable for approximating stream flow more accurately [27].

The work aims to create floodplain maps for three different return periods by combining the HEC-HMS and HEC-RAS models and using satellite-based PERSIANN precipitation records. The study's innovative approach is to evaluate hydrologic model accuracy using the coefficient of correlation (R-square) and use this to predict flow and generate a floodplain map. The resulting inundation map helps to illustrate changes in the floodplain across three different return period intervals. The study also compares it to the Federal Emergency Management Agency's (FEMA) floodplain map. The comparison computation of the inundation extent percentage aids in the evaluation of the risk factor. Finally, comparing values makes it easier to comprehend how climate change affects precipitation and creek flooding. The main objective of the study is to check the accuracy of the hydrologic model considering wet and dry season PERSIANN precipitation data and compare the 25-, 50-, and 100-year return periods floodplain with the FEMA. Although identical ungauged creeks can be mapped using the model under consideration, the precipitation data may vary depending on the location.

2. Study area

The river reach considered is Brush Creek, located in Missouri, US. Figure 1 shows the location map. Brush Creek is the tributary of the Blue River, which is the urban tributary. A major part of the land use around the creek covers approximately 10.02 km² of developed space for the commercial and residential areas. However, the total land use of the watershed and that around the study reach is 12.25 km^2 of developed open space, 23.43 km^2 of developed low intensity, 6.94 km^2 of developed medium intensity, 4.06 km^2 of developed high intensity, and 0.018 km^2 of pasture or hay. Table 1 shows the land use data. Figure 2 shows the land use map of the watershed and the area around the creek. The year considered for the initial phase of significant climate change by the IPCC is 1951, and catastrophic flash floods were seen in Brush Creek in 1977 and 1998.

The reach of the river considered for this study is in Jackson County. However, a major part of the watershed area is in Kansas State. Our study region is from Ward Parkway through Mission Woods (upstream side) to Frank A. Theis Park (downstream side). For the rivers section considered in the study, the upstream gauge station ID is 06893557, and the downstream gauge station ID is 06893557. The location of the upstream station is 94° 36' 19.4" W, 39° 11' 59.1" N, and the downstream station is 94° 34' 43.4" W, 39° 02' 21.3" N. The study reach is approximately 2.725 km long. On the upstream side, the watershed area is approximately 33.92 km^2. The flow and gauge height data from the downstream gauge stream aid in verifying the HEC-HMS and HEC-RAS models.

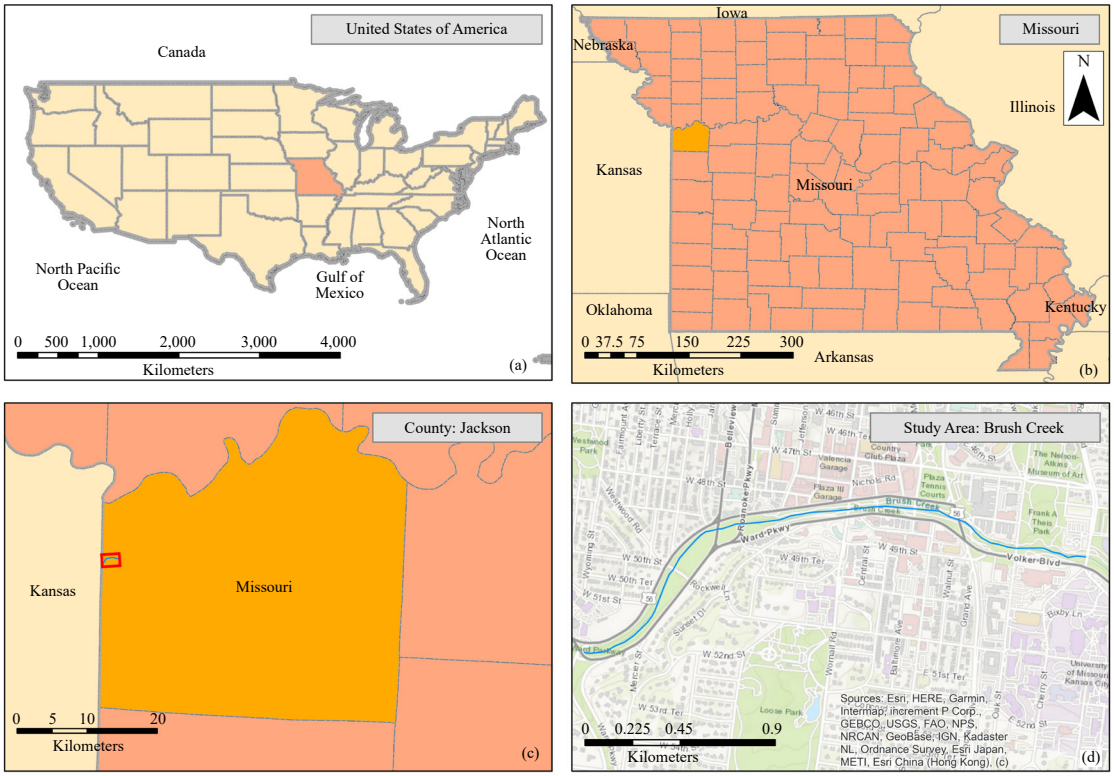

Figure 1. Study area map of the (a) country, (b) state, (c) county, and (d) river reach considered

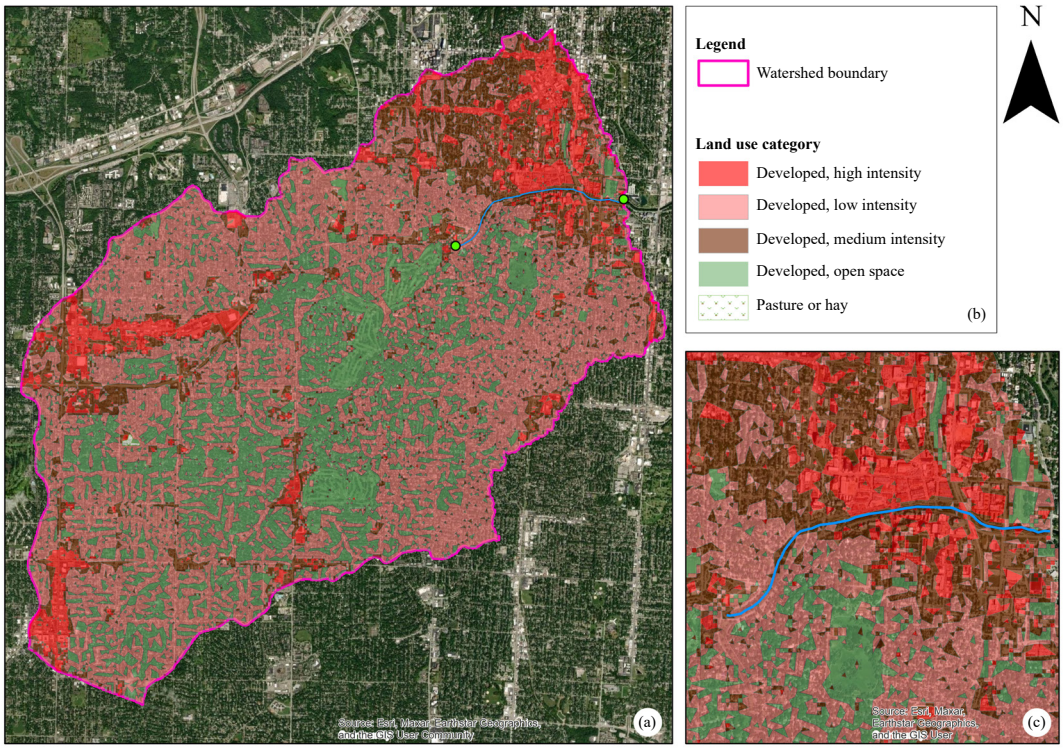

Figure 2. (a) Land use of the watershed, (b) map legend, and (c) land use around the study reach

Table 1. Total land use covered by watershed and that around the study reach considered

Grid code	Area (km^2)	Land use type
21	12.255	Developed, open space
22	23.431	Developed, low intensity
23	6.943	Developed, medium intensity
24	4.069	Developed, high intensity
81	0.018	Rangeland

3. Methodology

Although the work demonstrates an understanding of rainfall-runoff modelling in HEC-HMS and the creation of an inundation map using HEC-RAS, the watershed under consideration is an urbanising watershed without a meteorological station. As a result, the mathematical value of the inundation extent percentage is compared to the floodplain developed for 25-, 50-, and 100-year return periods. The subsections below provide a complete description of the methodology.

3.1 *PERSIANN precipitation data*

The PERSIANN system uses an algorithm that estimates the precipitation by combining infrared (IR) and passive/active microwave (PMW) sensor data from multiple satellites, like Geostationary Earth Orbiting (GEO) and Low Earth Orbit (LEO) satellites [28]. The PERSIANN system, created by the Centre for Hydrometeorology and Remote Sensing (CHRS), calculates the rainfall rate using an ANN function based on the 0.25° x 0.25°-pixel infrared, the brightness temperature image that is currently available from geostationary satellites [29]. The feature class of the watershed boundary is uploaded to the CHRS data site to gather rainfall data, and the results are produced in the format of NET. CDF. Considering the centroid of the watershed's latitude and longitude coordinates, the acquired file is extracted using Python code. The precipitation data was acquired in Excel and may now be used directly in the HEC-HMS model.

3.2 *Hydrologic modelling*

To create the model in HEC-HMS, first the files are created in the GIS using the extension Arc-Hydro Tools and Geospatial Hydrologic Modelling Extension (HEC-GeoHMS). The primary work for any hydrologic modelling involves the delineation of watersheds, and streams and extracting other common properties like drainage lines, outfall points, river length, slopes, flow path lines, and their characteristics. The data used are shown in Table 2.

Table 2. Data and its sources

Data	Sources
Watershed	Streamflow Statistics and Spatial Analysis Tools for Water-Resources Applications: USGS
Stream network	National Hydrography Dataset: USGS
Land use	Multi-Resolution Land Characteristics Consortium
Impervious layer	Multi-Resolution Land Characteristics Consortium
Soil data	Soil Survey Geographic Database (SSURGO)
Rainfall intensity	National Oceanic and Atmospheric Administration - Precipitation Frequency Data Server (NOAA-PFDS)

Note: USGS = United States Geological Survey

The detailed steps for rainfall-runoff simulation in HEC-HMS are described below.

3.2.1 *Terrain processing using Arc-Hydro Tools*

The extracted digital elevation mode (DEM) is converted into the required projected coordinate system if the coordinate system is not assigned. To refine the DEM more for analysis, it is reconditioned. The hydrologic parameters are extracted using the reconditioned DEM, and the final output required from this process is the drainage lines, the drainage outlet points, and the slope grid of the catchment. The detailed steps are shown in Figure 3.

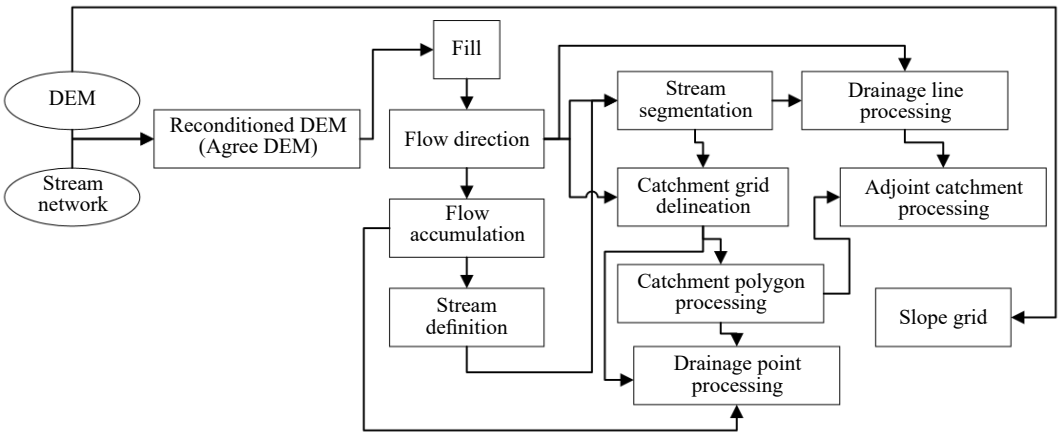

Figure 3. Terrain processing steps

3.2.2 *Basin processing using HEC-GeoHMS*

This involves creating the project area by defining the project point at the outlet point. Then the sub-basins are created. After that, it involves the determination of characteristic properties like river and basin slope, length, the longest flow path, and centroids. The major parameter to be determined in this process is the CN grid. The CN grid is obtained by merging land use and soil data. CN that is considered in past studies show that the runoff in any basin depends upon the type of vegetation around [30], which implies that current land use and soil data integration is necessary. The method based on which loss is calculated that involves the use of a CN grid is the Soil Conservation Service (SCS) method. The resulting CN grid is the file assigned along the CN related to soil type for specific land use types. The detailed steps are shown in Figure 4.

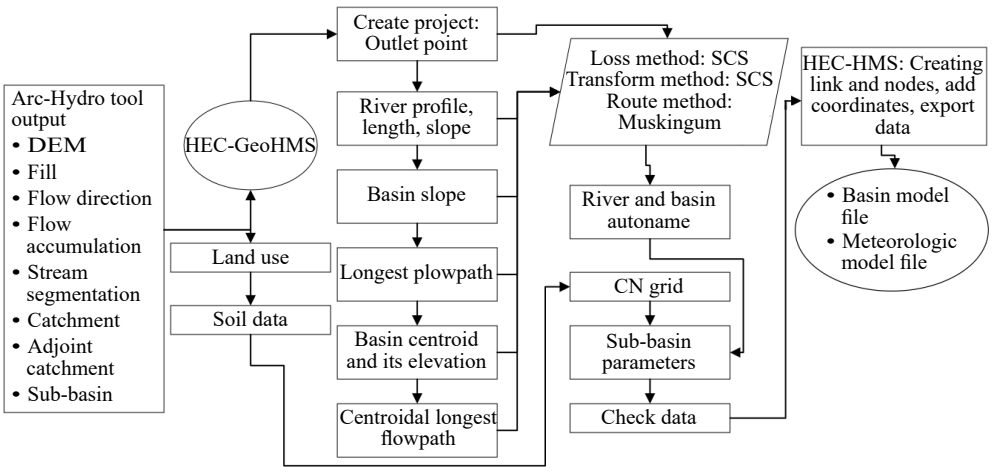

Figure 4. Basin processing steps and creating final files for HEC-HMS

3.2.3 *Model simulation in HEC-HMS*

The final exported files in GIS using HEC-GeoHMS are imported into the HEC-HMS model, i.e., importing the basin and the meteorological model. The major task before the simulation is creating the gauge parameter and assigning the precipitation data for the specific time interval. In HEC-HMS, the control specification includes the date and time interval of precipitation data added, i.e., the date and time of wet and dry season precipitation data considered. So, for the wet season event, hourly precipitation data is specified from July 22 to July 28, 2022, and for the dry season event, hourly precipitation data is specified from November 4 to November 6, 2022. The precipitation data extracted using Python code in the file from PERSIANN-CDR is the input to HEC-HMS and is a user-specified hyetograph. The SCS CN method is considered to estimate runoff, i.e., the CN grid, which is based on land use and soil type and developed using HEC-GeoHMS, is added to the HEC-HMS model. The next method is the Muskingum method, which uses k and x values and is the conservation of mass approach to route and inflow hydrographs. To compare the simulated flow with the observed flow value, the flow value extracted using USGS is specified as direct runoff in the model, and the method is called user-specified unit hydrograph. Then the flow of data for the same time interval is added to see the difference between the simulated data and the data from the USGS gauge station. Looking at the different parameters, the final decision will be based on whether the model is verified. After the validation, the model is run with the three different 25-, 50-, and 100-year return periods of rainfall from the National Oceanic and Atmospheric Administration (NOAA), which lead to the three different values of flow. The detailed steps are shown in Figure 5.

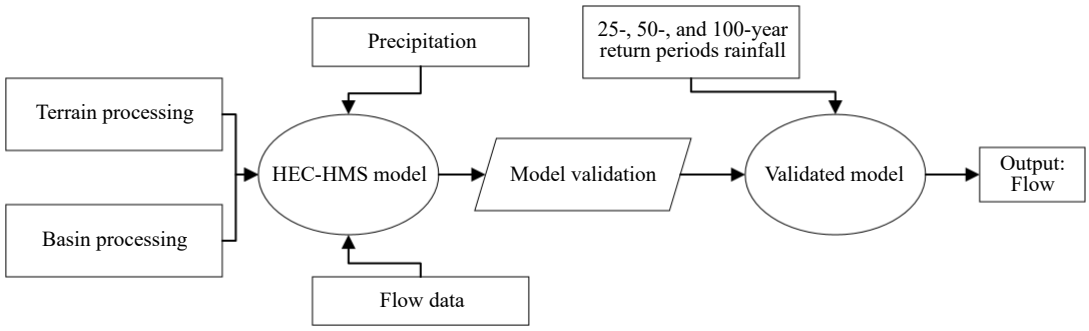

Figure 5. HEC-HMS model processing steps

3.3 *Hydraulic model*

The preparation of the floodplain mapping, or hydraulic modelling, is conducted in HEC-RAS. The simulation in HEC-RAS considers the mixed flow regime, i.e., the software analyses both subcritical and supercritical flow. The flow discharge is the regulated discharge obtained from the simulation in HEC-HMS. Thus, regulated discharge is the input in HEC-RAS and generates the flood plain area. The control specification in HEC-RAS is Manning's coefficient and river reach condition. The Manning's coefficient is assigned based on inbuilt features available in HEC-Geo-RAS. HEC-Geo-RAS shows the range of values accepted for Manning's coefficient according to the Multi-Resolution Land Characteristics Consortium (MRLC) land use data. The river reaches a boundary condition specifying that the channel considered for the study has a slope of 0.000038. The river centre lines, bank lines, flow path lines, and cross-sections are then constructed between the upstream and downstream gauge stations using the surface tools. Manning's coefficient is then assigned to every part of the cross-section in the geometric section. The flow is determined using the HEC-HMS model. The one dimensional inundation area is determined by steady flow analysis. The detailed steps are shown in Figure 6.

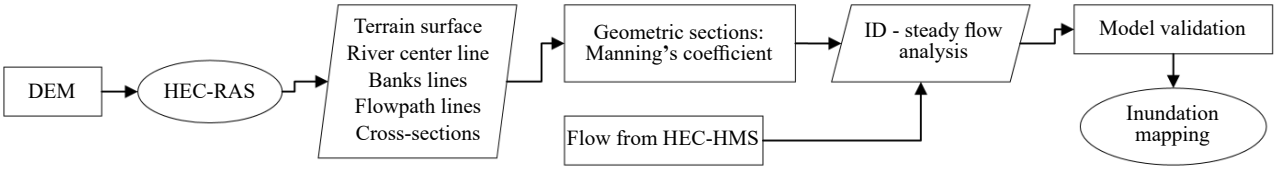

Figure 6. HEC-RAS modelling steps

Manning's coefficient is then assigned to every part of the cross-section depending upon the land use extracted from the MRLC viewer. The range of the allowable Manning's coefficient and the assigned value are shown in Table 3.

Table 3. Manning's coefficient allowable range and value considered

Land use	Allowable range	Assigned value
Developed, open space	0.030 - 0.050	0.030
Developed, low intensity	0.050 - 0.120	0.050
Developed, medium intensity	0.060 - 0.140	0.060
Developed, high intensity	0.080 - 0.200	0.080

3.4 *Model validation*

The validation of the HEC-HMS and HEC-RAS models involves checking similar values. The parameters considered for validation are Nash-Sutcliffe efficiency (*NSE*), root mean square (*RMSE*), percent bias (*PBIAS*), and standard deviation ratio (*RSR*). The values considered to be checked are $NSE \geq 0.65$, $PBIAS \leq \pm 10\%$, and $RSR \leq 0.60$ [31]. Table 4 shows the mathematical representation of the parameters considered for validation.

Table 4. Parameters with their mathematical interpretation used for calibration and validation

Parameters	Formula
Nash-Sutcliffe efficiency (*NSE*)	$1-\frac{\sum_{i=1}^{n}\left(R_o-R_c\right)^2}{\sum_{i=1}^{n}\left(R_o-R_{o,mean}\right)^2}$
Root mean square (*RMSE*)	$\sqrt{\frac{1}{n}\sum_{i=1}^{n}\left(R_o-R_c\right)^2}$
Percent bias (*PBIAS*)	$\frac{\sum_{i-1}^{n}\left(R_o-R_c\right)*100}{\sum_{i=1}^{n}R_o}$
Standard deviation ratio (*RSR*)	$\frac{RMSE}{Standard\ deviation}$

Note: R_o and R_c represent the data from USGS and the model, respectively; and $R_{o,\,mean}$ represents the mean of the R_o dataset

3.5 *Federal emergency management agency comparison*

The FEMA prepares the floodplain maps of the rivers and creeks. The study compares the floodplain generated by the FEMA and represents the increase or decrease in the floodplain area. Previous studies considered the validation of

the hydraulic model by comparing the flood area generated with FEMA [32, 33], but recently, the flow generated from recent precipitation data has exceeded the flood map produced by FEMA. So, the comparison passes the information through the research in different areas for making the proper emergency response plan to reduce the flood risk around the creeks and rivers [34].

3.6 *Calculation of inundation extent percentage*

The vulnerability of the rivers and creeks can be shown by calculating the percentage of inundation extent, which is the numerical representation obtained by comparing with FEMA. Equation 1 is used for the calculation of the inundation extent percentage. The relative difference in inundation extent can be directly obtained from the difference in the inundation area within two return periods, and the final value is expressed in terms of percentage [35].

$$\Delta IE_{1-F}(\%) = \frac{IE_F - IE_I}{IE_I} \times 100\% \quad (1)$$

IE_I represents the inundation area of the initial time period, and IE_F represents the inundation area of the subsequent time period considered. $\Delta IE_{I\text{-}F}$ is the inundation area change in the F return period as compared to the I return period. The computed values will be presented in the form of $IE_{25\text{-}50}$, $IE_{50\text{-}100}$, and $IE_{25\text{-}100}$.

4. Result and discussion

This section elucidates the alliance of the simulation output from HEC-HMS with the HEC-RAS model. This section focuses on model validation, output results from simulation, inundation floodplain maps, and the representation of inundation extent percentage. The detailed results are presented in the subsection below.

4.1 *HEC-HMS simulation and validation*

For the final simulation of the HEC-HMS model, the data on rainfall and flow are stored in model's control specifications in the precipitation gauge and flow gauge. The model validation considers both dry and wet seasons [36-38]. The data for the wet season ranges from July 22 to July 28, 2022, and the data for the dry season ranges from November 4 to November 6, 2022. Figures 7 (a) and (b) show the comparison of the simulated and observed runoff for both seasons. The simulated and observed peak runoff for the wet season is 28.55 and 26.04 m^3/s, respectively. The simulated and observed peak runoff for the dry season are 19.99 and 20.23 m^3/s, respectively. For the wet season, the values of the validation parameters are 0.68 for *NSE*, 3.01 for *RMSE*, -14% for *PBIAS*, and 0.55 for *RSR*. For the dry season, the values of the validation parameters are 0.77 for *NSE*, 2.5 for RMSE, -11% for *PBIAS*, and 0.35 for *RSR*. All the values are within the limit; hence, the model is verified for both wet and dry seasons [39]. So, the PERSIANN precipitation data is helpful in the hydrologic modelling of smaller creeks like Brush Creek for both seasons. The R-square values for the wet and dry seasons are 0.72 and 0.85, respectively. According to Gholami [40], to overcome the limitations of the calibration and validation of the model, the flood mapping will be more efficient by using the flood marks in the tree trunks. The precipitation depth from NOAA for 25-, 50-, and 100-year return periods is then used as input data in the model's frequency storm tab for the meteorological station defined. The simulation resulted in flow values of 260.51, 313.41, and 373.95 m^3/s for 25-, 50-, and 100-year return periods, respectively. The hydrograph for the three-return period is shown in Figure 8. This depicts the increase in flow as the return period precipitation value increases. The precipitation uncertainty resulted in a significant increment in flow value [41-43].

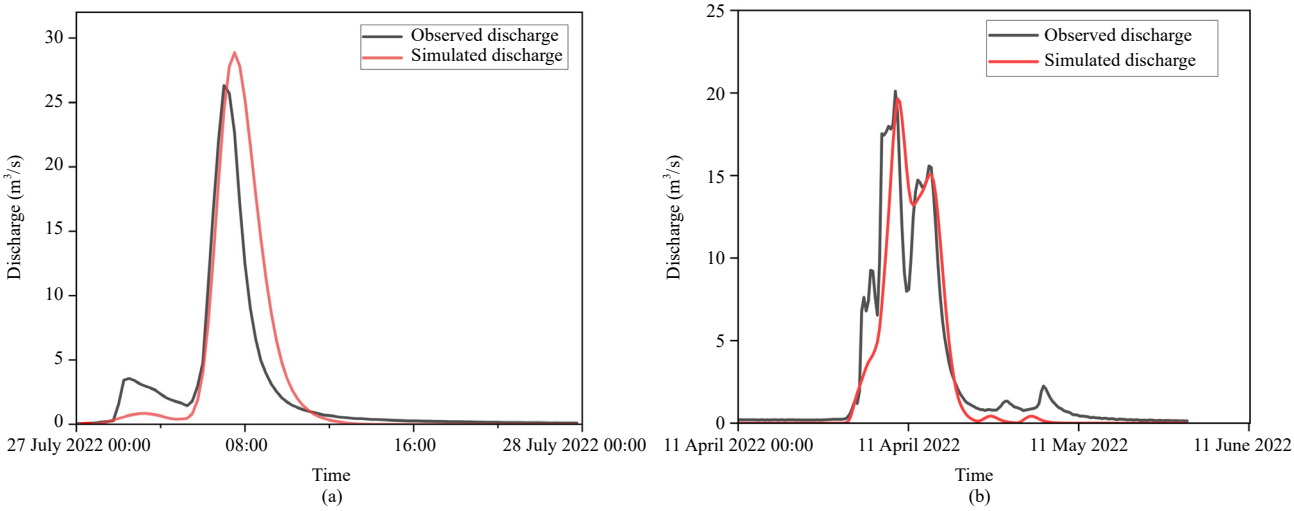

Figure 7. Observed and simulated discharge for (a) wet and (b) dry seasons

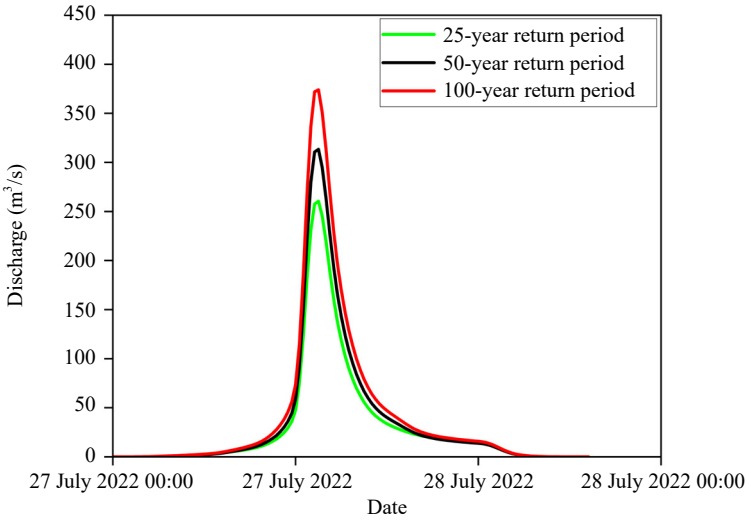

Figure 8. The hydrograph for the 25-, 50-, and 100-year return periods

4.2 *Inundation analysis from HEC-RAS*

At first, the simulation considers the known flow value from the USGS. Then the gauge height downstream from the USGS and the simulated model are considered for validation. The simulation and validation consider the flow values of 3.05, 2.74, 2.77, 1.86, and 2.52 m^3/s. These flow values are from different days. The flow has been observed, and the simulated gauge heights are 1.42, 1.42, 1.48, 1.35, and 1.64 metres and 1.45, 1.41, 1.42, 1.34, and 1.63 metres, respectively. The validation parameters calculated are 0.9 for NSE, 0.03 for RMSE, 0.82 for PBIAS, and 0.316 for RSR. These values are within the limit as discussed in the methodology section. Hence, the model is verified. The R-square value of the model is 0.96. The verified model is subjected to 25-, 50-, and 100-year return period flow values, which provide the inundation extent as shown in Figure 9. The outflow for 25-, 50-, and 100-year return periods is 260.51, 313.41, and 373.95 m^3/s, respectively. The inundation area for 25-, 50-, and 100-year return period flow values is 0.4, 0.42, and 0.44 km^2. The urban area affected by the three different return periods is 0.38, 0.4, and 0.42 km^2. The change in inundation extent indicates that the uncertainty in precipitation is causing the alteration in the flood regime. The maps show a clear view of the flood-risk areas. Moreover, the flow from the model verified using PERSIANN data

also predicts the flood regime, which will be helpful for the policymakers in the proper planning of the area around the creeks for urban expansion. Usually, city planners and policymakers define the area for artificial reservoirs or wetlands to control the flood regime after studying it [44], and it usually comes into action whenever the urbanisation expansion is rapid [45].

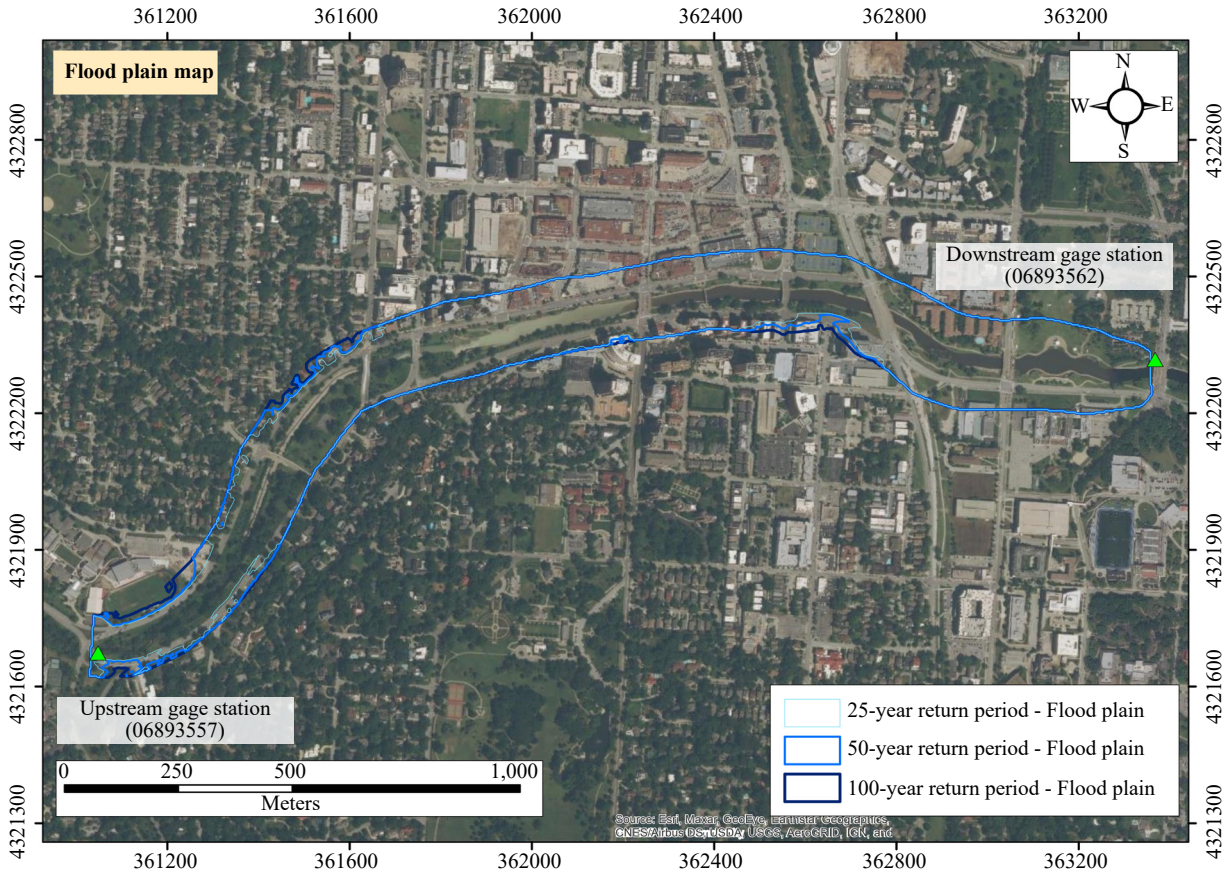

Figure 9. Map showing the floodplain area of three return period flood

4.3 *Comparison with FEMA*

The FEMA maps are readily available online and are open source. The FEMA maps show the regulatory floodway and the hazard area, which have a 1% annual chance of occurring. Response plans and safety measures are documented in the underlying FEMA flood hazard layers. But, due to climate change and abnormalities in the precipitation pattern, flooding is more likely to increase, even in the creeks [46]. The flash flood caused the river to rise up to the residential areas, and all the roads were blocked in the creek considered for this study in 2020. This study compares the FEMA map with the floodplain generated by considering the 100-year return period flow. The area under the floodplain is larger than that of FEMA. Furthermore, the model considers both season and average precipitation data to validate the model so that it can be used for predicting floods in any season and help prepare the emergency response plan. The floodplain area of the 100-year return period is remarkably large compared to FEMA, and the repetitive flash floods due to uncertain precipitation stipulate the need for water resources managers and policymakers to upgrade the safety scenario around such creeks and prevent more social, financial, and environmental loss [47]. The change in flood regime also highlights that the creeks and rivers whose floodplain is not in FEMA can be developed using a similar framework for the future emergency plan [48]. Figure 10 shows FEMA's comparison map of the floodplain area and the 100-year return period flood.

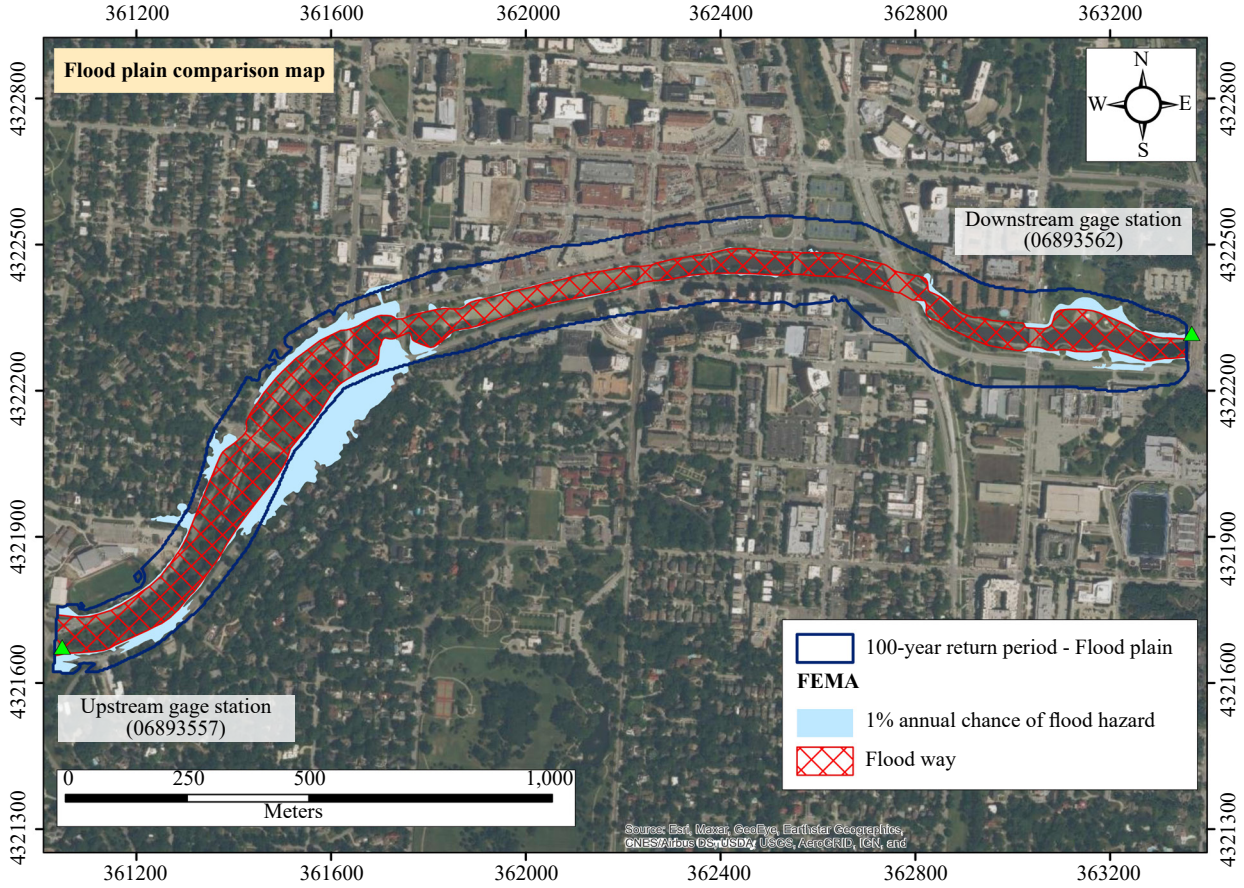

Figure 10. Floodplain comparison map of modelled flood and FEMA

4.4 *Inundation extent percentage*

The computed values for $IE_{25\text{-}50}$, $IE_{50\text{-}100}$, and $IE_{25\text{-}100}$ are shown in Table 5.

Table 5. Inundation extent percentage of 25-, 50-, and 100-year return period floodplain

Inundation extent percentage	$IE_{25\text{-}50}$	$IE_{50\text{-}100}$	$IE_{25\text{-}100}$
	5%	4.7%	10%

From 25- to 50-year return period, the inundation extent changes by 5%, from 50- to 100-year return period by 4.7%, and from 25- to 100-year return period by 10%. This suggests that the creek is in a mild flood-risk zone, and a flood may occur in the future. Therefore, this paper might be helpful for county planners in preparing quick response steps to avoid minor casualties and effectively manage urban expansion regions. According to a recent study, effective planning measures should be adopted in urban, semi-urban, and agricultural areas because the creeks are becoming more vulnerable. The contribution of this study is to provide the framework for developing the floodplain through the model, which is verified considering two-season precipitation data. If the gauge station is unavailable in the considered watershed, the gridded precipitation data can also be used [49-52]. Hence, the framework can be used similarly using PERSIANN data and verifying seasonally to provide a more convincing floodplain per requirements. The study leaves many unanswered questions and may consider various climate models and scenarios to better understand increasing flood regimes through future runoff projections. Additionally, future studies can focus on considering climate

model parameters like temperature, carbon emission scenarios, and wind speed to better represent the flood regime. Furthermore, validating a model by considering many seasonal data points to increase the model's effectiveness is also a good point to draw attention to for future research purposes.

5. Conclusions

The rivers and creeks, which were not vulnerable in the past, have started to give warning signs due to flash flood events caused by altered precipitation patterns. Different climate-related research documents the change in the precipitation pattern caused by the warmer climate. As a result, the floodplain, considering the recent precipitation data and also in the summer, is covering a greater extent of the landscape around rivers and creeks. So, before developing the floodplain model for rainfall-runoff, the model is verified considering the precipitation data of both wet and dry seasons around Brush Creek. For PERSIANN-CDR, the gridded precipitation data is used when the gauge station is unavailable in the considered watershed. Thus, the result in the model is verified by the R-square value of 0.72 for the wet season and 0.84 for the dry season. Therefore, the study infers that the precipitation data from both seasons depicts the projection of the floodplain in the present climatic scenario. Moreover, the parameters considered for validation suggest that the model has higher accuracy when using the dry season data rather than the wet season data. The study also provides insights on the change in floodplain considering 25-, 50-, and 100-year retention period precipitation data. The study compares the geospatial representation of the flood inundation simulated by the hydraulic model. The simulated runoff value gradually increases considering recent data, and the change in floodplain area is also gradually increasing with a difference of 0.02 km^2. Although this difference in the increase in the inundation area is not high, calculating the inundation extent percentage shows that the change is 10% between floodplains from 25- to 100-year return periods. So, the creek is now on the verge of a mild vulnerable zone. Hence, the current scenario suggests that policymakers and planners should consider this zone for developing further emergency response plans and be prepared for the future, as the reports highlight the rapid increase in temperature in a few decades and a warmer climate causing more abnormalities in the rainfall pattern. Furthermore, the geospatial comparison of the 100-year return period flood and the FEMA flood zone shows that the floodplain covers developed areas. So, the study also supports updating the flood-prone zone developed considering recent precipitation data and updating mitigation measures to overcome any uncertain casualties in the future.

Acknowledgement

The authors would like to thank the University of Illinois System (Award #107688) for providing research support for the current study. All analyses use publicly available datasets.

Conflict of interest

There is no conflict of interest for this study.

References

[1] Field CB, Barros VR, Dokken DJ, Mach KJ, Mastrandrea MD, Bilir TE, et al. (eds.) *Climate Change 2014: Impacts, Adaptation, and Vulnerability Part A: Global and Sectoral Aspects*. United States of America: Cambridge University Press; 2014. https://www.ipcc.ch/site/assets/uploads/2018/02/WGIIAR5-PartA_FINAL.pdf

[2] Tamaddun K, Kalra A, Ahmad S. Identification of streamflow changes across the continental United States using variable record lengths. *Hydrology*. 2016; 3(2): 1-21. https://doi.org/10.3390/hydrology3020024

[3] Sagarika S, Kalra A, Ahmad S. Evaluating the effect of persistence on long-term trends and analyzing step changes in streamflows of the continental United States. *Journal of Hydrology*. 2014; 517: 36-53. https://doi.org/10.1016/

j.jhydrol.2014.05.002
[4] Mallakpour I, Villarini G. The changing nature of flooding across the central United States. *Nature Climate Change*. 2015; 5: 250-254. https://doi.org/10.1038/nclimate2516
[5] Kalra A, Ahmad S, Nayak A. Increasing streamflow forecast lead time for snowmelt-driven catchment based on large-scale climate patterns. *Advances in Water Resources*. 2013; 53: 150-162. https://doi.org/10.1016/j.advwatres.2012.11.003
[6] Shadkam S, Ludwig F, van Oel P, Kirmit Ç, Kabat P. Impacts of climate change and water resources development on the declining inflow into Iran's Urmia Lake. *Journal of Great Lakes Research*. 2016; 42(5): 942-952. https://doi.org/10.1016/j.jglr.2016.07.033
[7] Maheshwari BL, Simmons BL, Singh VP. Role and complexity of integrated water-resources management for periurban landscapes in Australia. *Journal of Hydrologic Engineering*. 2012; 17(2): 229-236. https://doi.org/10.1061/(ASCE)HE.1943-5584.0000471
[8] Dhakal KP, Chevalier LR. Urban stormwater governance: The need for a paradigm shift. *Environmental Management*. 2016; 57: 1112-1124. https://doi.org/10.1007/s00267-016-0667-5
[9] Martínez-Paz JM, Gomariz-Castillo F, Pellicer-Martínez F. Appraisal of the water footprint of irrigated agriculture in a semi-arid area: The Segura River Basin. *PLoS One*. 2018; 13: 1-20. https://doi.org/10.1371/journal.pone.0206852
[10] Thakur B, Parajuli R, Kalra A, Ahmad S, Gupta R. Coupling HEC-RAS and HEC-HMS in precipitation runoff modelling and evaluating flood plain inundation map. In: Dunn CN, Weele BV. (eds.) *World environmental and water resources congress 2017*. Reston, Virginia: American Society of Civil Engineers; 2017. p.240-251. https://doi.org/10.1061/9780784480625.022
[11] Gholami V, Asghari A, Salimi ET. Flood hazard zoning using geographic information system (GIS) and HEC-RAS model (case study: Rasht City). *Caspian Journal of Environmental Sciences*. 2016; 14(3): 263-272. https://cjes.guilan.ac.ir/article_1862.html
[12] Ashouri H, Hsu KL, Sorooshian S, Braithwaite DK, Knapp KR, Cecil LD, et al. PERSIANN-CDR: Daily precipitation climate data record from multisatellite observations for hydrological and climate studies. *Bulletin of the American Meteorological Society*. 2015; 96(1): 69-83. https://doi.org/10.1175/BAMS-D-13-00068.1
[13] Miao C, Ashouri H, Hsu KL, Sorooshian S, Duan Q. Evaluation of the PERSIANN-CDR daily rainfall estimates in capturing the behavior of extreme precipitation events over China. *Journal of Hydrometeorology*. 2015; 16(3): 1387-1396. https://doi.org/10.1175/JHM-D-14-0174.1
[14] Aghakouchak A, Behrangi A, Sorooshian S, Hsu K, Amitai E. Evaluation of satellite-retrieved extreme precipitation rates across the Central United States. *Journal of Geophysical Research: Atmospheres*. 2011; 116(D2): 1-11. https://doi.org/10.1029/2010JD014741
[15] Kalra A, Paudel S, Wang Y, Acharya A, Joshi N, Gupta R. Application of the HEC-HMS model for runoff simulation of big muddy river, Illinois. In: Pierson J, Grubert E. (eds.) *World environmental and water resources congress 2022: Adaptive planning and design in an age of risk and uncertainty, June 5-8, 2022, Atlanta, Georgia*. Reston, Virginia: American Society of Civil Engineers; 2022. p.481-491. https://doi.org/10.1061/9780784484258.044
[16] Kalra A, Joshi N, Baral S, Pradhan SN, Mambepa M, Paudel S, et al. Coupled 1D and 2D HEC-RAS floodplain modeling of Pecos River in New Mexico. In: Baldwin LA, Gude VG. *World environmental and water resources congress 2021: Planning a resilient future along America's freshwaters. June 7-11, 2021, Virtual Conference*. Reston, Virginia: American Society of Civil Engineers; 2021. p.165-178. https://doi.org/10.1061/9780784483466.016
[17] Ndeketeya A, Dundu M. Application of HEC-HMS model for evaluation of rainwater harvesting potential in a semi-arid city. *Water Resources Management*. 2021; 35: 4217-4232. https://doi.org/10.1007/s11269-021-02941-0
[18] Chea S, Oeurng C. Flow Simulation in an ungauged catchment of Tonle Sap Lake Basin in Cambodia: Application of the HEC-HMS model. *Water Utility Journal*. 2017; 17: 3-17. https://www.semanticscholar.org/paper/Flow-simulation-in-an-ungauged-catchment-of-Tonle-%3A-Chea-Oeurng/b298c6636df4acbb2aeac805edee608014714dc8
[19] Haile AT, Tefera FT, Rientjes T. Flood forecasting in Niger-Benue basin using satellite and quantitative precipitation forecast data. *International Journal of Applied Earth Observation and Geoinformation*. 2016; 52: 475-484. https://doi.org/10.1016/j.jag.2016.06.021
[20] Bhandari M, Nyaupane N, Mote SR, Kalra A, Ahmad S. 2D unsteady routing and flood inundation mapping for lower region of Brazos River Watershed. In: Dunn CN, Weele BV. (eds.) *World environmental and water resources congress 2017: Hydraulics and waterways and water distribution systems analysis*. Reston, Virginia: American

Society of Civil Engineers; 2017. p.292-303. https://doi.org/10.1061/9780784480625.027
[21] Aryal A, Acharya A, Kalra A. Assessing the implication of climate change to forecast future flood using CMIP6 climate projections and HEC-RAS modeling. *Forecasting*. 2022; 4(3): 582-603. https://doi.org/10.3390/forecast4030032
[22] Shrestha A, Rahaman MM, Kalra A, Thakur B, Lamb KW, Maheshwari P. Regional climatological drought: An assessment using high-resolution data. *Hydrology*. 2020; 7(2): 1-25. https://doi.org/10.3390/hydrology7020033
[23] Joshi N, Kalra A, Lamb KW. Land–ocean–atmosphere influences on groundwater variability in the South Atlantic–Gulf Region. *Hydrology.* 2020; 7(4): 1-28. https://doi.org/10.3390/hydrology7040071
[24] Thakur B, Kalra A, Joshi N, Jogineedi R, Thakali R. Analyzing the impacts of serial correlation and shift on the streamflow variability within the climate regions of contiguous United States. *Hydrology*. 2020; 7(4): 1-19. https://doi.org/10.3390/hydrology7040091
[25] Bhusal A, Parajuli U, Regmi S, Kalra A. Application of machine learning and process-based models for rainfall-runoff simulation in DuPage River Basin, Illinois. *Hydrology*. 2022; 9(7): 1-20. https://doi.org/10.3390/hydrology9070117
[26] Gholami V, Sahour H. Simulation of rainfall-runoff process using an artificial neural network (ANN) and field plots data. *Theoretical and Applied Climatology*. 2021; 147: 87-98. https://doi.org/10.1007/s00704-021-03817-4
[27] Kalra A, Ahmad S. Estimating annual precipitation for the Colorado River Basin using oceanic-atmospheric oscillations. *Water Resources Research*. 2012; 48(6): 1-24. https://doi.org/10.1029/2011WR010667
[28] Sorooshian S, Hsu KL, Gao X, Gupta HV, Imam B, Braithwaite D. Evaluation of PERSIANN system satellite-based estimates of tropical rainfall. *Bulletin of the American Meteorological Society*. 2000; 81(9): 2035-2046. https://doi.org/10.1175/1520-0477(2000)081%3C2035:EOPSSE%3E2.3.CO;2
[29] Nguyen P, Shearer EJ, Tran H, Ombadi M, Hayatbini N, Palacios T, et al. The CHRS Data Portal, an easily accessible public repository for PERSIANN global satellite precipitation data. *Scientific Data*. 2019; 6: 1-10. https://doi.org/10.1038/sdata.2018.296
[30] Gholzom EH, Gholami V. A comparison between natural forests and reforested lands in terms of runoff generation potential and hydrologic response (case study: Kasilian Watershed). *Soil and Water Research*. 2012; 7(4): 166-173. https://doi.org/10.17221/18/2012-SWR
[31] Moriasi DN, Arnold JG, Liew MWV, Bingner RL, Harmel RD, Veith TL. Model evaluation guidelines for systematic quantification of accuracy in watershed simulations. *American Society of Agricultural and Biological Engineers*. 2007; 50(3): 885-900. https://doi.org/10.13031/2013.23153
[32] Afshari S, Tavakoly AA, Rajib MA, Zheng X, Follum ML, Omranian E, et al. Comparison of new generation low-complexity flood inundation mapping tools with a hydrodynamic model. *Journal of Hydrology*. 2018; 556: 539-556. https://doi.org/10.1016/j.jhydrol.2017.11.036
[33] Jafarzadegan K, Merwade V, Saksena S. A geomorphic approach to 100-year floodplain mapping for the conterminous United States. *Journal of Hydrology*. 2018; 561: 43-58. https://doi.org/10.1016/j.jhydrol.2018.03.061
[34] Shao W, Xian S, Lin N, Kunreuther H, Jackson N, Goidel K. Understanding the effects of past flood events and perceived and estimated flood risks on individuals' voluntary flood insurance purchase behavior. *Water Research*. 2017; 108: 391-400. https://doi.org/10.1016/j.watres.2016.11.021
[35] Mohanty MP, Simonovic SP. Changes in floodplain regimes over Canada due to climate change impacts: Observations from CMIP6 models. *Science of the Total Environment*. 2021; 792: 1-15. https://doi.org/10.1016/j.scitotenv.2021.148323
[36] Boongaling CGK, Faustino-Eslava DV, Lansigan FP. Modeling land use change impacts on hydrology and the use of landscape metrics as tools for watershed management: The case of an ungauged catchment in the Philippines. *Land Use Policy*. 2018; 72: 116-128. https://doi.org/10.1016/j.landusepol.2017.12.042
[37] Azmat M, Qamar MU, Huggel C, Hussain E. Future climate and cryosphere impacts on the hydrology of a scarcely gauged catchment on the Jhelum river basin, Northern Pakistan. *Science of the Total Environment*. 2018; 639: 961-976. https://doi.org/10.1016/j.scitotenv.2018.05.206
[38] Akter A, Ahmed S. Potentiality of rainwater harvesting for an urban community in Bangladesh. *Journal of Hydrology*. 2015; 528: 84-93. https://doi.org/10.1016/j.jhydrol.2015.06.017
[39] Sahraei S, Asadzadeh M, Unduche F. Signature-based multi-modelling and multi-objective calibration of hydrologic models: Application in flood forecasting for Canadian prairies. *Journal of Hydrology*. 2020; 588: 125095. https://doi.org/10.1016/j.jhydrol.2020.125095
[40] Gholami V. Prediction of flood discharge and flood flow depth using a hydraulic model and flood marks on the trees in ungauged forested watersheds. *Journal for Forest Science*. 2022; 68(5): 190-198. https://doi.org/10.17221/6/2022-JFS

[41] Arnell NW, Reynard NS. The effects of climate change due to global warming on river flows in Great Britain. *Journal of Hydrology*. 1996; 183(3-4): 397-424. https://doi.org/10.1016/0022-1694(95)02950-8
[42] Novotny EV, Stefan HG. Stream flow in Minnesota: Indicator of climate change. *Journal of Hydrology*. 2007; 334(3-4): 319-333. https://doi.org/10.1016/j.jhydrol.2006.10.011
[43] Ficklin DL, Luo Y, Luedeling E, Zhang M. Climate change sensitivity assessment of a highly agricultural watershed using SWAT. *Journal of Hydrology*. 2009; 374(1-2): 16-29. https://doi.org/10.1016/j.jhydrol.2009.05.016
[44] Barbier EB, Acreman M, Knowler D. *Economic Valuation of Wetlands: A Guide for Policy Makers and Planners*. Gland, Switzerland: Ramsar Convention Bureau; 1997. https://www.researchgate.net/publication/246010067_Economic_valuation_of_wetlands_a_guide_for_policy_makers_and_planners
[45] Lebel L, Manuta JB, Garden P. Institutional traps and vulnerability to changes in climate and flood regimes in Thailand. *Regional Environmental Change*. 2011; 11: 45-58. https://doi.org/10.1007/s10113-010-0118-4
[46] Silvestro F, Rebora N, Giannoni F, Cavallo A, Ferraris L. The flash flood of the Bisagno Creek on 9th October 2014: An "unfortunate" combination of spatial and temporal scales. *Journal of Hydrology*. 2016; 541: 50-62. https://doi.org/10.1016/j.jhydrol.2015.08.004
[47] Tockner K, Stanford JA. Riverine flood plains: Present state and future trends. *Environmental Conservation*. 2002; 29(3): 308-330. https://doi.org/10.1017/S037689290200022X
[48] Samela C, Manfreda S, Troy TJ. Dataset of 100-year flood susceptibility maps for the continental U.S. derived with a geomorphic method. *Data in Brief*. 2017; 12: 203-207. https://doi.org/10.1016/j.dib.2017.03.044
[49] Komi K, Neal J, Trigg MA, Diekkrüger B. Modelling of flood hazard extent in data sparse areas: A case study of the Oti River basin, West Africa. *Journal of Hydrology: Regional Studies*. 2017; 10: 122-132. https://doi.org/10.1016/j.ejrh.2017.03.001
[50] Ahiablame L, Chaubey I, Engel B, Cherkauer K, Merwade V. Estimation of annual baseflow at ungauged sites in Indiana USA. *Journal of Hydrology*. 2013; 476: 13-27. https://doi.org/10.1016/j.jhydrol.2012.10.002
[51] Reed S, Schaake J, Zhang Z. A distributed hydrologic model and threshold frequency-based method for flash flood forecasting at ungauged locations. *Journal of Hydrology*. 2007; 337(3-4): 402-420. https://doi.org/10.1016/j.jhydrol.2007.02.015
[52] Xue X, Hong Y, Limaye AS, Gourley JJ, Huffman GJ, Khan SI, et al. Statistical and hydrological evaluation of TRMM-based multi-satellite precipitation analysis over the Wangchu Basin of Bhutan: Are the latest satellite precipitation products 3B42V7 ready for use in ungauged basins? *Journal of Hydrology*. 2013; 499: 91-99. https://doi.org/10.1016/j.jhydrol.2013.06.042